foods

MDPI

Article

Cellar Age and Spatial Position Shape Nitrogen Partitioning and Bacterial Differentiation in Strong-Flavor Baijiu Pit Muds

Tianyao Han [1,2], Zongze Li [3], Min Sun [3], Huai Chen [1,4], Bo Deng [3,*] and Dan Xue [1,*]

[1] Mountain Ecological Restoration and Biodiversity Conservation Key Laboratory of Sichuan Province, Chengdu Institute of Biology, Chinese Academy of Sciences, Chengdu 610213, China
[2] University of Chinese Academy of Sciences, Beijing 100049, China
[3] National Engineering Research Center of Solid-state Brewing, Luzhou Laojiao Group Co., Ltd., Luzhou 646000, China
[4] College of Resources and Environment, Aba Teachers University, Aba 624000, China
* Correspondence: dengbo@lzlj.com (B.D.); xuedan@cib.ac.cn (D.X.)

Abstract

Nitrogen supports microbial biosynthesis, yet how its partitioning relates to microbial and metabolic differentiation across pit mud habitats remains unclear. We characterized physicochemical properties, extracellular enzyme activities, and bacterial, fungal, and archaeal communities in samples from the upper wall, lower wall, and bottom of strong-flavor Baijiu cellars aged 4, 40, and 100 years. Bottom total nitrogen concentrations in older cellars were 2.06–2.20 times those in young cellars, but microbial biomass nitrogen (MBN) was 66.5–66.7% lower. Bottom biomass C:N increased from 5.54 to 8.86 and 13.96 across the three age groups. Bottom *Lactobacillus* relative abundance declined from 29.85% to 1.15–2.34%, accompanied by greater *Proteiniphilum*, *Petrimonas* and *Sedimentibacter* relative abundances. Bacterial composition was concordant with bottom metabolite profiles (Procrustes $M^2 = 0.383$, $p = 0.0001$, $q < 0.001$). Carbohydrate and sugar phosphate were higher in young bottom mud. Older bottom mud showed higher signals for putatively annotated homocystine and lower signals for serine, threonine, guanine and deoxyuridine monophosphate. Partial least squares path modeling (PLS-PM) indicated that variation in selected metabolites in bottom pit mud may be associated with nitrogen status and microbial community characteristics. These findings distinguish bulk nitrogen enrichment from microbial biomass nitrogen status and identify candidate measurements for characterizing young and older pit mud.

Keywords: microbial biomass stoichiometry; microbial community composition; extracellular enzymes; untargeted metabolomics; fermentation ecology

Check for updates

Academic Editor: Moktar Hamdi

Received: 27 October 2026
Revised: 18 November 2026
Accepted: 25 November 2026
Published: 27 November 2026

Copyright: © 2026 by the authors. Licensee MDPI, Basel, Switzerland. This article is an open access article distributed under the terms and conditions of the Creative Commons Attribution (CC BY) license.

1. Introduction

Pit mud supports microorganisms that produce and transform organic acids during strong-flavor Baijiu fermentation. These acids contribute to sensory properties and provide precursors for ester formation [1]. Studies combining community profiling and genome reconstruction have associated cellar age with microbial specialization, hydrolytic potential, and organic acid metabolism [2]. Qian et al. [3] combined fermentation profiling with simulated fermentation experiments and demonstrated that acetate and lactate produced by fermented grain communities could be converted into butyrate and hexanoate by pit mud microorganisms. The resources supporting these functions also vary within fermentation cellars. Understanding pit mud development therefore requires consideration of nutrient conditions and microbial properties across both cellar ages and spatial positions.

Nitrogenous substrates supply nitrogen for biosynthesis and, in some cases, carbon for energy metabolism, linking microbial biomass formation with fermentation metabolism. Defined pit mud cultures have demonstrated nutritional complementarity involving organic acids, with integrated omics suggesting additional exchange involving amino acid resources [4]. Depth-resolved metagenomics has further linked pit mud maturation to amino acid metabolic potential and hydrogen-transfer networks involving methanogens [5]. In Jiang-flavor Baijiu fermentation, Wei et al. [6] associated variation in amino acid concentrations with fungal community assembly and demonstrated that serine promoted the growth and ethanol production of *Zygosaccharomyces bailii*. Together, these studies motivate examining nitrogenous resources alongside carbon availability and community composition in pit mud.

Nitrogen concentrations and microbial biomass represent distinct aspects of nitrogen status. Total nitrogen (TN) reflects the bulk nitrogen pool, total dissolved nitrogen (TDN) reflects the extractable fraction, and microbial biomass nitrogen (MBN) reflects the biomass pool; these three are complementary but distinct aspects of nitrogen status [7]. Microbial biomass carbon (MBC) and nitrogen (MBN), together with MBC:MBN, describe biomass elemental pools and composition, which differ from those of bulk soil [8]. Soil isotope tracing further demonstrates that nitrogen derived from microbial residues can persist in mineral associated fractions outside living biomass [9]. In pit mud, differences in ammonium among cellar age groups have been reported without significant differences in TN [10]. These observations highlight the importance of distinguishing bulk nitrogen concentration, TDN, and nitrogen represented in microbial biomass. Spatial heterogeneity provides an additional context for interpreting these relationships. Studies of pit mud layers and cellar age groups have documented differences in community composition and predicted carbon and nitrogen metabolic functions [11]. In fermented grains, bacterial communities, organic acids, and volatile metabolites also vary with distance from pit mud [12]. These findings indicate that cellar age should be considered alongside sampling position when relating nutrient conditions to microbial properties. However, it remains unclear whether TN and TDN concentrations correspond consistently to microbial biomass across cellar positions, and how these relationships coincide with community differentiation and nonvolatile metabolite profiles at the pit bottom.

To understand how nitrogen partitioning relates to microbial and metabolic differentiation in pit mud, we compared nitrogen pools, microbial biomass stoichiometry, and bacterial, fungal, and archaeal communities across the upper wall, lower wall, and bottom of 11 cellars spanning three age classes. These measurements were interpreted alongside the physicochemical properties and potential extracellular enzyme activities of each habitat, complemented by elemental analysis and nonvolatile metabolite profiling of matched bottom samples. Our analysis centered on three interconnected questions: (i) do TN and TDN concentrations, microbial biomass C and N, and biomass C:N exhibit concordant patterns across cellar ages and sampling positions; (ii) which shifts in bacterial, fungal, and archaeal community composition accompany these nitrogen and biomass patterns, and which environmental factors are associated with these shifts; and (iii) how are nitrogen status and microbial community composition related to nonvolatile metabolite profiles in bottom pit mud, particularly individual nitrogenous compounds? This study may help distillery personnel responsible for fermentation management and pit mud maintenance evaluate nitrogen enrichment together with microbial biomass nitrogen status. The resulting candidate measurements could inform monitoring at different cellar positions and the design of maintenance trials to support fermentation stability.

2. Materials and Methods

2.1. Sample Collection

Pit mud (PM) samples were collected in 2024 from a strong-flavor Baijiu distillery in Luzhou, Sichuan, China (28.87° N, 105.56° E). Eleven cellars were randomly selected from different locations within the workshop, including five 4-year cellars, three 40-year cellars, and three 100-year cellars. PM was collected from the upper wall (T), lower wall (L), and bottom (B) of each cellar. At each position, three spatially separated subsamples (200 g each) were pooled and homogenized into one composite sample. The composite samples were placed in sterile bags immediately after collection and transported on ice. In the laboratory, aliquots for microbial community analysis and for metabolomics of bottom pit mud were transferred to −80 °C within 24 h of collection. Material for extracellular enzyme assays was kept refrigerated. Fresh pit mud was used for water content and dissolved organic carbon measurements. A separate portion for routine physicochemical analyses, including total carbon and total nitrogen, was air-dried indoors away from direct sunlight, ground, passed through a 0.25 mm sieve, mixed, and stored in sealed containers. Each composite sample represents one position within one cellar and was prepared by pooling three spatial subsamples.

2.2. Detection of Physicochemical Properties and Enzyme Activity of PM

Water content (WC) was determined by oven drying at 105 °C to constant mass (DHG-9240A, Shanghai Yiheng Scientific Instrument Co., Ltd., Shanghai, China) and expressed on a dry mass basis. Ash content was determined gravimetrically after ignition at 600 °C in an SGM M12LZ-1200 muffle furnace (Sigma (Shanghai) High-Temperature Electric Furnace, Shanghai, China), using a modified dry ashing procedure [13]. Total carbon (TC) and total nitrogen (TN) were measured by dry combustion using an elemental analyzer (vario MACRO cube, Elementar, Langenselbold, Germany) [14]. Humic acid (HA) was determined using an adapted procedure based on GB/T 34766–2017 [15]. Samples were extracted with alkaline sodium pyrophosphate, and the extract was acidified to pH 1 to precipitate HA. The precipitate was redissolved in NaOH and analyzed by dichromate oxidation followed by titration with ferrous ammonium sulfate.

DOC was determined using the water extraction approach described by Wang et al. [16], adapted for fresh pit mud. Samples were mixed with deionized water at a ratio of 1:5 (w/v) and shaken at 200 rpm for 30 min at room temperature. The suspension was centrifuged at 4000 rpm for 10 min, and the supernatant was filtered through a 0.45 μm membrane. DOC in the filtrate was measured using a total organic carbon analyzer (Vario TOC cube, Elementar, Langenselbold, Germany). Total dissolved nitrogen (TDN) was extracted with 2 mol L^{-1} KCl (1:5, w/v) for 1 h and determined after oxidative digestion at 100 °C for 90 min, with absorbance measured at 220 and 275 nm. Reagent blanks received the same oxidant addition and digestion treatment.

Total phenolics (TPM) were extracted from 1 g of pit mud with 30 mL of 1 mol L^{-1} NaOH, and water-soluble phenolics (DPM) were extracted from 5 g of pit mud with 30 mL of deionized water. Both suspensions were shaken at 200 rpm for 4 h, centrifuged at 3000 rpm for 10 min, and filtered through a 0.45 μm membrane. Color was developed in the dark for 1 h, and the filtrates were quantified using a modified Folin–Ciocalteu assay at 750 nm [17]. An optical index of organic matter decomposition (DOD) was determined using a modified alkaline extraction and colorimetric method based on Wang et al. [18]. Samples were extracted with 8% NaOH, and absorbance was measured at 400 nm.

Microbial biomass carbon (MBC) and nitrogen (MBN) were determined using modified chloroform fumigation–extraction methods [19,20]. Fumigated and unfumigated samples were extracted with 0.5 mol L^{-1} K_2SO_4 at a soil to solution ratio of 1:4 and filtered

through medium speed filter paper. Extractable carbon and nitrogen were measured using a liquiTOC II analyzer (Elementar, Langenselbold, Germany). MBC and MBN were calculated from the differences between fumigated and unfumigated extracts using kEC = 0.45 and kEN = 0.54, respectively. Microbial biomass C:N was calculated as MBC/MBN for each sample on a mass basis; group means and SD were then calculated from these individual ratios.

The activities of acid phosphatase (AP), β-1,4-glucosidase (BG), cellobiohydrolase (CBH), β-1,4-N-acetylglucosaminidase (NAG), phenol oxidase (POX) and peroxidase (PER) were measured following Saiya-Cork et al. [21]. Pit mud (1.5–2 g) was dispersed in 100 mL of 50 mM sodium acetate buffer (pH 5.0). Hydrolytic assays used 4-methylumbelliferyl phosphate, 4-methylumbelliferyl β-D-glucoside, 4-methylumbelliferyl β-D-cellobioside and 4-methylumbelliferyl N-acetyl-β-D-glucosaminide for AP, BG, CBH and NAG, respectively. AP and NAG were incubated in the dark for 2 h, and BG and CBH for 5 h, in black 96-well plates. Fluorescence was read at excitation and emission wavelengths of 365 and 450 nm within 2 min of adding NaOH to terminate the reaction. Oxidative assays used L-DOPA, with H_2O_2 included for PER, followed by 4 h of dark incubation and absorbance measurement at 460 nm. Assays were performed under standardized aerobic conditions and measure potential activities.

Elemental concentrations in bottom pit mud were determined by ICP-OES (Optima 8300, PerkinElmer, Waltham, MA, USA) following H_2SO_4–$HClO_4$ digestion.

2.3. Metabolomic Analysis of PM

Cold methanol extraction was adapted for bottom pit mud with reference to the sample preparation approach described by Yuan et al. [22]. The extraction solvent consisted of prechilled 80% methanol (precooled to −20 °C) containing 0.1% formic acid.

UHPLC–MS/MS analysis was performed using a Vanquish UHPLC system coupled to a Q Exactive HF Orbitrap mass spectrometer (Thermo Fisher Scientific, Scientific, Waltham, MA, USA). Chromatographic separation was achieved on a Hypersil GOLD C18 (Thermo Fisher Scientific, Waltham, MA, USA) column (100 × 2.1 mm, 1.9 μm) maintained at 40 °C, with a flow rate of 0.2 mL min^{-1} and an injection volume of 5 μL. In positive ion mode, mobile phase A was 0.1% formic acid in water; in negative ion mode, it was 5 mM ammonium acetate at pH 9.0. Methanol served as mobile phase B in both modes. The gradient was programmed as follows: 2% B at 0–1.5 min, 85% B at 3.0 min, 100% B at 10.0 min, and 2% B at 10.1 min, maintained until 12.0 min.

Data were acquired in positive and negative electrospray ionization modes over an m/z range of 100–1500, with data-dependent MS/MS acquisition. The spray voltage was 3.5 kV. The sheath gas and auxiliary gas settings were 35 and 10 arbitrary units, respectively. The capillary temperature was 320 °C, the auxiliary gas heater temperature was 350 °C, and the S-lens RF level was 60.

Pooled quality control (QC) samples were prepared by combining equal-volume aliquots from all samples, processed alongside the experimental samples, and interspersed throughout the analytical sequence to monitor analytical stability. Raw data were processed using Compound Discoverer 3.1, with blank samples used to remove background signals and total peak area used for normalization. Features with QC coefficients of variation < 30% were retained. Metabolites were annotated using mzCloud/mzVault or MassList, corresponding to levels 2 and 3, respectively, according to the service provider's classification.

2.4. DNA Extraction and Sequencing

Total genomic DNA was extracted from pit mud samples using the E.Z.N.A.® Soil DNA Kit (Omega Bio-tek, Norcross, GA, USA). The bacterial 16S rRNA gene (V1–V9), the fungal ITS region, and the archaeal 16S rRNA gene were amplified with barcoded primer pairs 27F/1492R (27 cycles), ITS1F/ITS4R (32 cycles), and A1F/1490R (29 cycles), respectively; the bacterial primer pair was provided by Biozeron Biotechnology Co., Ltd. (Shanghai, China). Purified amplicons were pooled in equimolar amounts, used to construct SMRTbell libraries, and sequenced on a PacBio Sequel platform. Circular consensus sequences (CCS) were generated with SMRT Link v9.0, requiring a minimum of three full passes and a predicted accuracy of at least 99%. After demultiplexing, barcode/primer trimming, quality and domain-specific length filtering, and UCHIME chimera removal, sequences were independently clustered within each domain into OTUs at 98.65% identity using UPARSE v7.1. Bacterial and archaeal OTUs were classified using the RDP Classifier [23] against SILVA SSU132; fungal OTUs were annotated against UNITE. The taxonomic confidence threshold was set to 70%.

2.5. Statistical Analysis

Statistical analyses were performed using R (v 4.4.1) within the Positron integrated development environment (Posit Software, v 2025.12.1; Posit Software, PBC, Boston, MA, USA). Physicochemical properties, enzyme activities, and alpha diversity were analysed with restricted maximum likelihood linear mixed models, with age, position, and their interaction as fixed effects and a random intercept for cellar; fixed effects were tested using Type III Kenward–Roger F tests. Genus proportions were arcsine-square-root transformed before fitting the same model structure. Age comparisons within each property and position were Holm-adjusted across the three age comparisons, and BH adjustment across the 20 age tests is reported as a sensitivity analysis. Bottom elemental concentrations were compared by one-way ANOVA with Holm-adjusted age comparisons per element, with Welch tests as a sensitivity analysis.

Community variation was described with weighted UniFrac PCoA and genus-level RDA. PERMANOVA age tests exchanged intact cellar profiles (the three positions together) among age groups, with cellar identity as the error denominator; position was tested with residual permutations within cellars. PERMDISP used bias-adjusted distances among cellar centroids. Bonferroni correction was applied across the six alpha diversity responses for each effect. Procrustes tests used permutations of intact cellar profiles for environmental comparisons, preserving the spatial correspondence, and unrestricted permutations for the bottom-only comparisons; probabilities were BH-adjusted across the three domains within each comparison.

Genus–environment Spearman probabilities were BH-adjusted across all 6880 tests in the three domains. Co-occurrence graphs pooled the spatial samples within each age group. Genera were retained if they occurred in at least 60% of samples and averaged at least 0.1% relative abundance in at least one spatial position; edges required $|\rho| > 0.80$ and $p < 0.01$, followed by K-core ≥ 3 filtering. Zi–Pi roles were calculated on the broader unfiltered graphs using unweighted Louvain modules in igraph [24] and were interpreted as exploratory topological classifications. Genus–metabolite network edges required $|\rho| \geq 0.60$ and $p < 0.05$.

Community assembly was assessed using the Sloan neutral community model [25] and an abundance-weighted βNTI/RCbray null-model framework, with assembly processes classified according to established criteria [26,27]. Phylogenetic trees were constructed using FastTree 2.1.3 [28].

Positive- and negative-ion metabolomic data were combined for OPLS-DA in SIMCA 14.1. Differential metabolite candidates were selected using two-sided Welch's t-tests on $\log_2$-transformed intensities, with $|\log_2 FC| \geq 1$ and unadjusted $p < 0.05$. Benjamini–Hochberg-adjusted p values were additionally calculated within each comparison. VIP scores from separate PLS-DA models were used for volcano-plot visualization.

Random forest regression used randomForest and rfPermute, with 1000 trees and 100 response permutations for predictor importance. PLS-PM used plspm to examine associations among cellar age, elemental concentrations, nitrogen status, selected genera and selected metabolites in matched bottom samples [29]. Path coefficients and effect decomposition were exported from the same fitted model. Uncertainty was summarized using 2000 bootstrap resamples.

3. Results

3.1. Age-Associated Variation and Spatial Heterogeneity in Pit Mud Physicochemical Properties

Significant differences in pit mud physicochemical properties were detected among different cellar ages and across spatial positions (Table 1). pH showed age ($p = 0.018$) and age × position effects ($p = 0.042$), and WC showed an age effect ($p = 0.021$). TC increased towards the bottom within each group and showed a position effect ($p = 0.004$), but no significant age effect ($p = 0.083$). TN and TDN concentrations were higher in both older groups across positions; their age effects were significant ($p = 0.024$ and $p = 0.014$, respectively). TN also showed a position effect ($p = 0.007$). MBC was higher in older mud at the upper wall and in young mud at the lower wall and bottom, with a position effect ($p = 0.023$) and an age × position interaction ($p < 0.001$). MBN was lower in both older groups at all three positions and showed an age effect ($p < 0.001$). Microbial C:N increased across the age groups at the bottom; the highest ratio was recorded at the upper wall of 40-year cellars (34.84 ± 2.29). Age, position and their interaction affected biomass C:N (all $p < 0.001$). DOC was lowest at the upper wall and showed a position effect ($p = 0.002$). Ash showed age ($p = 0.025$) and position effects ($p = 0.001$). Age effects were also detected for DOD ($p = 0.005$), TPM ($p = 0.032$) and DPM ($p = 0.025$). No significant age effects were detected for the potential enzyme activities.

Bottom elemental patterns differed among groups (Figure S1). The pairwise comparisons indicated higher P, Ca, Mn, and Cu in 40-year cellars than in 4-year cellars and lower Cu in 100-year cellars than in 40-year cellars ($p < 0.05$). P concentrations showed the largest proportional differences: NA and NB concentrations were 11.89 and 14.91 times the 4-year cellars. Ca and Mg were higher, and Na and Mo lower, in the 40-year and 100-year cellars as descriptive trends. No significant pairwise differences were detected for Mg, Zn, Ni, Fe, Na, Mo, or K.

Table 1. Physicochemical properties and extracellular enzyme activities of pit muds across cellar ages and spatial positions (mean ± SD).

Property	4 Years			40 Years			100 Years			*p*		
	T	L	B	T	L	B	T	L	B	Age	Position	Age × Position
pH	5.93 ± 0.44 ^{b}	6.00 ± 0.44 ^{a}	5.51 ± 0.12 ^{b}	6.67 ± 0.28 ^{a}	6.17 ± 0.11 ^{a}	6.47 ± 0.30 ^{a}	6.27 ± 0.05 ^{ab}	6.22 ± 0.10 ^{a}	6.31 ± 0.45 ^{a}	**0.018**	0.196	**0.042**
WC (%)	20.18 ± 4.06 ^{b}	17.72 ± 2.80 ^{b}	20.14 ± 3.56 ^{a}	30.07 ± 6.44 ^{a}	22.04 ± 3.36 ^{ab}	23.39 ± 6.77 ^{a}	26.17 ± 1.73 ^{ab}	26.72 ± 7.17 ^{a}	23.39 ± 3.32 ^{a}	**0.021**	0.174	0.359
TC ($g \cdot kg^{-1}$)	34.82 ± 11.51 ^{a}	40.56 ± 7.98 ^{a}	59.29 ± 25.65 ^{a}	49.16 ± 27.81 ^{a}	86.90 ± 27.17 ^{a}	99.13 ± 20.05 ^{a}	60.20 ± 34.72 ^{a}	68.67 ± 33.52 ^{a}	87.40 ± 38.01 ^{a}	0.083	**0.004**	0.541
DOC ($mg \cdot kg^{-1}$)	12.61 ± 4.89 ^{a}	14.12 ± 2.36 ^{a}	26.34 ± 10.14 ^{a}	9.84 ± 4.76 ^{a}	27.57 ± 3.51 ^{a}	30.10 ± 10.78 ^{a}	19.29 ± 8.67 ^{a}	27.04 ± 12.76 ^{a}	23.76 ± 13.79 ^{a}	0.429	**0.002**	0.083
MBC ($mg \cdot kg^{-1}$)	1186.67 ± 729.71 ^{b}	2369.55 ± 578.86 ^{a}	1617.88 ± 530.17 ^{a}	2377.02 ± 289.79 ^{a}	493.57 ± 131.00 ^{b}	862.02 ± 164.11 ^{a}	2025.11 ± 515.68 ^{ab}	1080.03 ± 196.06 ^{b}	1354.87 ± 192.88 ^{a}	0.115	**0.023**	**<0.001**
TN ($g \cdot kg^{-1}$)	6.57 ± 1.91 ^{a}	7.91 ± 1.85 ^{a}	7.79 ± 2.29 ^{b}	10.01 ± 5.59 ^{a}	14.87 ± 4.23 ^{a}	17.17 ± 2.14 ^{a}	10.42 ± 5.18 ^{a}	11.70 ± 3.43 ^{a}	16.01 ± 6.75 ^{a}	**0.024**	**0.007**	0.270
TDN ($mg \cdot kg^{-1}$)	3.82 ± 1.05 ^{a}	3.80 ± 1.35 ^{b}	3.26 ± 0.86 ^{b}	5.39 ± 1.57 ^{a}	5.39 ± 1.22 ^{ab}	6.44 ± 1.03 ^{a}	5.06 ± 0.82 ^{a}	6.20 ± 1.53 ^{a}	7.13 ± 1.47 ^{a}	**0.014**	0.102	0.068
MBN ($mg \cdot kg^{-1}$)	316.00 ± 91.64 ^{a}	315.98 ± 102.37 ^{a}	290.28 ± 18.65 ^{a}	68.41 ± 9.54 ^{b}	168.92 ± 47.25 ^{b}	96.77 ± 6.49 ^{b}	128.59 ± 25.64 ^{b}	60.88 ± 9.45 ^{c}	97.18 ± 11.92 ^{b}	**<0.001**	0.734	0.215
Microbial C:N	3.68 ± 1.69 ^{c}	7.64 ± 0.58 ^{b}	5.54 ± 1.60 ^{b}	34.84 ± 2.29 ^{a}	3.02 ± 0.81 ^{c}	8.86 ± 1.07 ^{ab}	16.15 ± 5.36 ^{b}	18.37 ± 6.27 ^{a}	13.96 ± 1.21 ^{a}	**<0.001**	**<0.001**	**<0.001**
Ash (%)	11.78 ± 2.49 ^{a}	12.73 ± 1.33 ^{b}	16.07 ± 5.12 ^{b}	16.82 ± 6.27 ^{a}	27.65 ± 6.96 ^{a}	27.51 ± 6.67 ^{a}	17.10 ± 5.72 ^{a}	18.14 ± 5.53 ^{ab}	24.03 ± 7.64 ^{ab}	**0.025**	**0.001**	0.125
HA (%)	0.79 ± 1.04 ^{a}	2.21 ± 1.99 ^{a}	3.37 ± 3.66 ^{a}	0.52 ± 0.29 ^{a}	1.03 ± 0.56 ^{a}	3.95 ± 0.11 ^{a}	2.43 ± 1.58 ^{a}	1.19 ± 0.88 ^{a}	1.56 ± 1.29 ^{a}	0.868	0.110	0.303
DOD	0.04 ± 0.01 ^{a}	0.04 ± 0.01 ^{b}	0.06 ± 0.02 ^{b}	0.10 ± 0.06 ^{a}	0.15 ± 0.05 ^{a}	0.18 ± 0.06 ^{a}	0.11 ± 0.06 ^{a}	0.13 ± 0.10 ^{a}	0.14 ± 0.06 ^{ab}	**0.005**	0.089	0.707

Table 1. *Cont.*

Property	4 Years			40 Years			100 Years			*p*		
	T	L	B	T	L	B	T	L	B	Age	Position	Age × Position
TPM ($mg \cdot g^{-1}$)	24.32 ± 3.69 ^{b}	21.50 ± 4.40 ^{b}	24.72 ± 5.62 ^{a}	37.78 ± 9.67 ^{a}	26.80 ± 3.21 ^{ab}	29.62 ± 8.11 ^{a}	30.30 ± 5.40 ^{ab}	33.00 ± 8.11 ^{a}	25.33 ± 3.26 ^{a}	**0.032**	0.206	0.178
DPM ($mg \cdot g^{-1}$)	9.74 ± 1.20 ^{b}	8.69 ± 1.60 ^{a}	9.41 ± 1.58 ^{a}	13.93 ± 3.73 ^{a}	10.55 ± 1.80 ^{a}	11.40 ± 3.35 ^{a}	12.03 ± 0.40 ^{ab}	12.47 ± 3.81 ^{a}	11.42 ± 1.56 ^{a}	**0.025**	0.352	0.619
AP ($nmol \cdot g^{-1} \cdot h^{-1}$)	34.20 ± 19.47 ^{a}	57.15 ± 49.20 ^{a}	104.33 ± 84.82 ^{a}	25.70 ± 24.26 ^{a}	26.73 ± 18.90 ^{a}	13.92 ± 7.48 ^{b}	11.58 ± 16.64 ^{a}	30.45 ± 21.15 ^{a}	8.82 ± 5.16 ^{b}	0.053	0.579	0.282
BG ($nmol \cdot g^{-1} \cdot h^{-1}$)	40.66 ± 20.27 ^{a}	63.74 ± 36.09 ^{a}	44.06 ± 37.92 ^{a}	46.39 ± 7.91 ^{a}	44.92 ± 7.94 ^{a}	54.55 ± 28.86 ^{a}	59.58 ± 26.30 ^{a}	49.99 ± 21.47 ^{a}	55.10 ± 20.52 ^{a}	0.914	0.920	0.565
CBH ($nmol \cdot g^{-1} \cdot h^{-1}$)	4.00 ± 3.80 ^{a}	13.98 ± 4.96 ^{a}	70.98 ± 83.99 ^{a}	5.05 ± 4.51 ^{a}	29.95 ± 29.74 ^{a}	10.97 ± 2.13 ^{a}	8.97 ± 2.50 ^{a}	13.54 ± 5.32 ^{a}	5.31 ± 4.93 ^{a}	0.444	0.329	0.162
NAG ($nmol \cdot g^{-1} \cdot h^{-1}$)	54.48 ± 31.34 ^{a}	155.63 ± 56.55 ^{a}	354.11 ± 283.16 ^{a}	71.08 ± 49.97 ^{a}	204.53 ± 125.53 ^{a}	96.18 ± 23.69 ^{b}	85.44 ± 22.29 ^{a}	117.89 ± 6.96 ^{a}	61.48 ± 39.18 ^{b}	0.280	0.132	0.052
POX ($\mu mol \cdot g^{-1} \cdot h^{-1}$)	1.13 ± 1.85 ^{a}	0.13 ± 0.16 ^{a}	0.67 ± 0.38 ^{a}	0.72 ± 0.37 ^{a}	0.27 ± 0.36 ^{a}	0.83 ± 0.48 ^{a}	0.62 ± 0.65 ^{a}	0.16 ± 0.11 ^{a}	0.28 ± 0.17 ^{a}	0.695	0.232	0.921
PER ($\mu mol \cdot g^{-1} \cdot h^{-1}$)	3.58 ± 4.56 ^{a}	0.62 ± 0.55 ^{a}	1.86 ± 1.36 ^{a}	1.43 ± 0.55 ^{a}	0.64 ± 0.90 ^{a}	1.97 ± 0.96 ^{a}	1.82 ± 1.38 ^{a}	0.83 ± 0.61 ^{a}	1.19 ± 0.49 ^{a}	0.633	0.239	0.762

Note: T, upper wall; L, lower wall; B, pit bottom. WC, water content; HA, humic acid; TC, total carbon; TN, total nitrogen; DOC, dissolved organic carbon; TDN, total dissolved nitrogen; TPM, total phenolic; DPM, dissolved phenolic, DOD, degree of decomposition; MBC, microbial biomass carbon; MBN, microbial biomass nitrogen; AP, acid phosphatase; BG, β-1,4-glucosidase; CBH, cellobiohydrolase; NAG, β-1,4-N-acetylglucosaminidase; POX, phenol oxidase; PER, peroxidase. Values are means ± SD across independent cellars, with five cellars in the 4-year group, three in the 40-year group and three in the 100-year group. Each cellar contributed one composite sample per spatial position, prepared by pooling three spatial subsamples. Within each property and spatial position, means without a shared lowercase superscript letter differ among ages at Holm-adjusted $p < 0.05$. Holm adjustment covers the three age comparisons within each property and position; letters are not compared across positions. The final three columns report nominal Type III Kenward–Roger tests of age, position and their interaction from models with a random intercept for cellar. Significant differences are in bold ($p < 0.05$).

3.2. Diversity and Composition of Bacterial, Fungal and Archaeal Communities

Bacterial Shannon diversity showed an age × position interaction ($p < 0.001$), with bottom values of 4.07 ± 0.38 in 4-B, 5.91 ± 0.37 in 40-B and 6.06 ± 0.22 in 100-B (Figure S2A). Chao1 richness showed no significant age, position or interaction effects in any of the three domains. Neither fungal nor archaeal Shannon diversity showed significant effects of age, position or their interaction (Figure S2B,C).

Bacterial compositional differences among cellar age groups depended on sampling position (Figure 1A). Age × position interactions were detected for *Lactobacillus*, *Proteiniphilum*, *Sedimentibacter*, *Prevotella*, *Petrimonas*, *Hydrogenispora* and *Thermobrachium* (Table S1). At the pit bottom, *Lactobacillus* relative abundance decreased from 29.85% in 4-B to 1.15% in 40-B and 2.34% in 100-B, accompanied by higher relative abundances of *Proteiniphilum*, *Sedimentibacter* and *Petrimonas* in both older groups. Upper wall *Prevotella* relative abundance decreased from 10.40% in 4-year cellars to 5.45% in 40-year cellars and 0.57% in 100-year cellars. *Anaerocella* showed a position effect ($p = 0.032$); both *Anaerocella* and *Hydrogenispora* were most abundant at the lower wall in 4-year cellars.

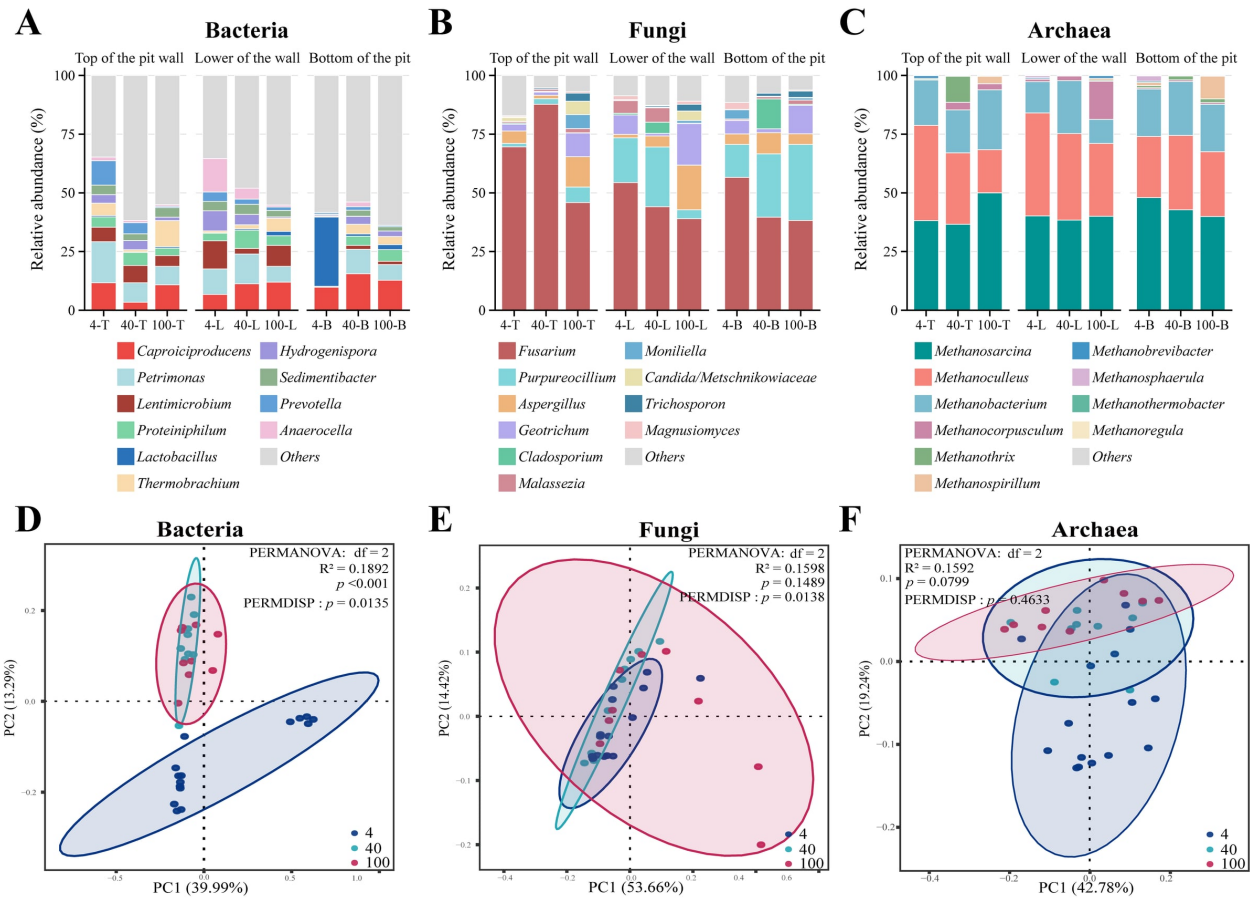

Figure 1. Taxonomic composition and community structure of the pit mud microbiome across cellar ages and sampling positions. Genus level relative abundance of bacterial (**A**), fungal (**B**) and archaeal (**C**) genera in upper wall, lower wall and bottom pit mud. Principal coordinates analysis (PCoA) of bacterial (**D**), fungal (**E**) and archaeal (**F**) communities based on weighted UniFrac distances. Age effects were assessed by PERMANOVA with whole-cellar permutation, and dispersion by PERMDISP on the cellar centroids. T, L and B denote the upper wall, lower wall and bottom, respectively.

Fungal communities were dominated by *Fusarium*, which showed a position effect ($p = 0.003$) and reached its highest relative abundance in 40-T (Figure 1B). Its bottom relative

abundance was 56.76% in 4-B, 39.75% in 40-B and 38.30% in 100-B. *Purpureocillium* showed a position effect ($p < 0.001$) and an age × position interaction ($p = 0.041$), with bottom relative abundances of 14.07%, 27.03% and 32.48% in 4-B, 40-B and 100-B, respectively. *Aspergillus* also showed an age × position interaction ($p = 0.001$). No significant age main effects were detected for fungal (Table S1).

Archaeal communities were dominated by *Methanosarcina*, *Methanoculleus* and *Methanobacterium*, none of which showed significant age, position or interaction effects (Figure 1C).

Bacterial PCoA showed clearer separation of 4-year cellars from 40-year and 100-year cellars, with substantial overlap between the two older groups. Cellar age was associated with bacterial community structure in PERMANOVA (weighted UniFrac, $R^2 = 0.1892$, $p < 0.001$; Figure 1D). Fungal and archaeal communities overlapped substantially, and their overall age effects were not significant (fungi: $R^2 = 0.1598$, $p = 0.1489$; archaea: $R^2 = 0.1592$, $p = 0.0799$; Figure 1E,F). Bacterial composition also varied with position ($p = 0.0001$) and showed an age × position interaction ($p = 0.0006$). Fungal composition varied with position ($p = 0.0037$). Dispersion among cellar centroids differed by age for bacteria ($p = 0.0135$) and fungi ($p = 0.0138$), but no significant dispersion difference was detected for archaea ($p = 0.4633$).

3.3. Microbial Co-Occurrence Network Topology and Community Assembly Patterns

Microbial co-occurrence networks contained fewer nodes and edges across the three cellar age groups. The 4-year cellar network contained 80 nodes and 715 edges (Figure 2A), decreasing to 71 nodes and 272 edges in 40-year cellars (Figure 2B) and 61 nodes and 145 edges in 100-year cellars (Figure 2C). Modularity increased from 0.210 in 4-year cellars to 0.517 in 40-year cellars and 0.657 in 100-year cellars. Average path length increased correspondingly from 2.040 to 3.064 and 4.743. Positive associations predominated in all three networks, accounting for 56.36%, 60.66%, and 58.62% of edges in 4-year cellars, 40-year cellars, and 100-year cellars, respectively.

Zi–Pi analysis identified *Bradyrhizobium* and *Mesorhizobium* among the connectors in 4-year cellars, with no module or network hubs detected (Figure 2D). In 40-year cellars, *Herbivorax*, *Duncaniella*, and *Lysinibacillus* were classified as module hubs, and *Aminobacterium* and *Fusarium* were connectors (Figure 2E). In 100-year cellars, *Desulfofundulus* was a module hub, and connectors included *Aminipila*, *Aspergillus*, and *Methanobrevibacter* (Figure 2F).

Neutral community model fits differed among microbial domains (Figure S3A). Bacterial R^2 increased from 0.114 in 4-year cellars to 0.232 in 40-year cellars and 0.290 in 100-year cellars, although model fit remained limited. Fungal fit was weak in 4-year cellars ($R^2 = 0.127$) and negative in 40-year cellars and 100-year cellars. Archaeal R^2 values were 0.513, 0.148, and 0.451 in 4-year cellars, 40-year cellars, and 100-year cellars, respectively, showing no consistent trend across cellar-age groups.

Null model analysis based on βNTI and RCbray identified heterogeneous selection as the predominant process across all bacterial sample pairs, accounting for 64.4%, followed by undominated processes (17.6%) and dispersal limitation (16.9%). Homogenizing dispersal and homogeneous selection each accounted for less than 1%. Within individual age and position groups, bacterial βNTI exceeded 2 in all comparisons at the lower wall of 40-year cellars, corresponding to 100% heterogeneous selection. All comparisons in 40-T were classified as dispersal limitation. Heterogeneous selection accounted for 66.7% of comparisons in 100-T but only 33.3% in 100-B, where undominated processes were more frequent (66.7%) (Figure S3B). Fungal turnover was predominantly classified as undominated, accounting for 89.0% of all sample pairs. Heterogeneous and homogeneous selection contributed 10.6% and 0.4%, respectively. Within individual age–position groups, heterogeneous selection

was detected only at the lower wall of 4-year cellars (30.0%) and 100-year cellars (33.3%). All comparisons in the remaining groups were classified as undominated (Figure S3C). Archaeal βNTI values remained between −2 and 2 in all spatial comparisons. Across all sample pairs, undominated processes (55.7%) and dispersal limitation (41.7%) accounted for most archaeal turnover. Dispersal limitation was particularly frequent at the lower wall of 40-year cellars, contributing 66.7% of within-group comparisons (Figure S3D).

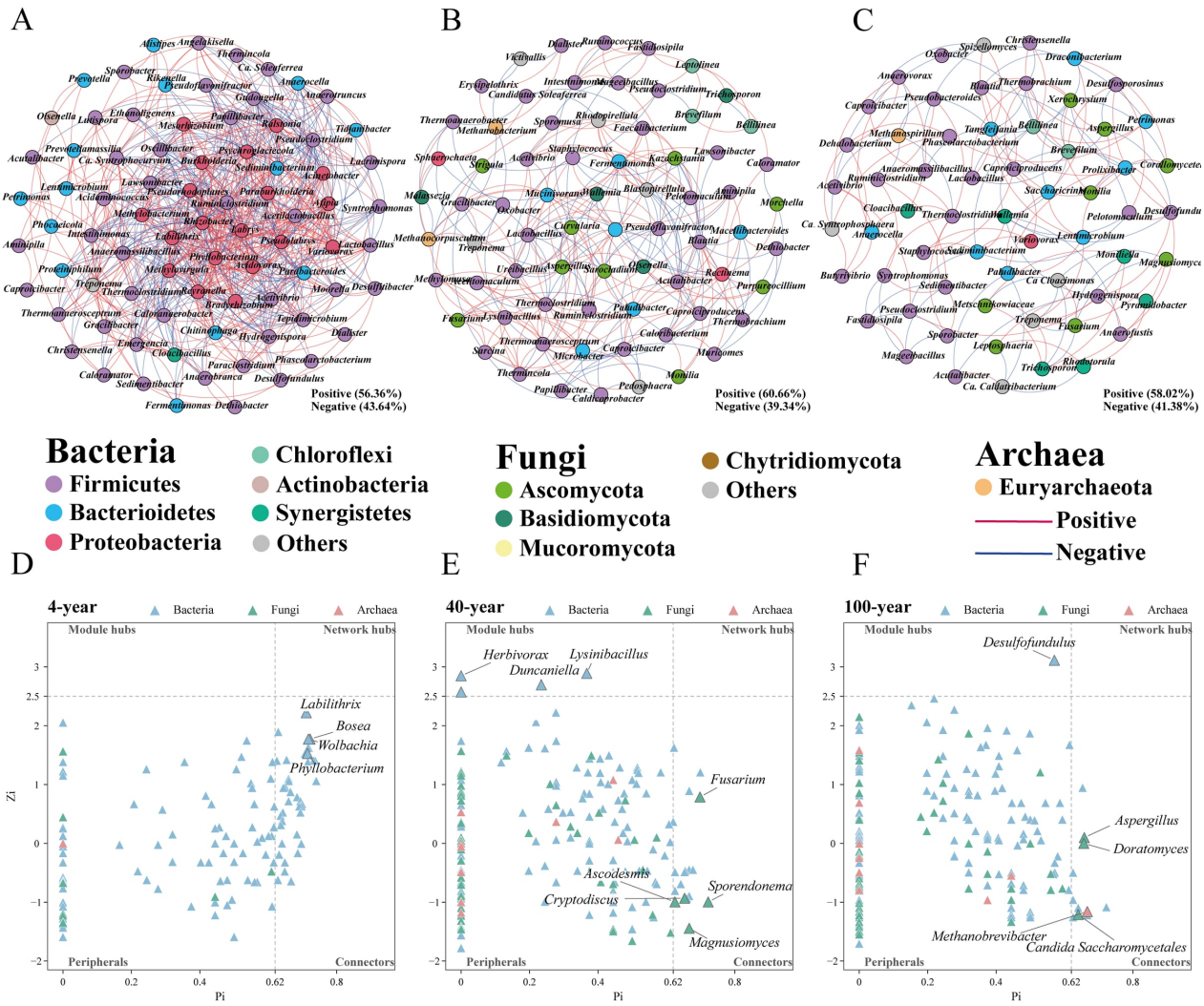

Figure 2. Exploratory co-occurrence patterns and topological roles of microbial genera in pit mud across cellar ages. (**A**–**C**) Co-occurrence networks of bacterial, fungal, and archaeal genera in (**A**) 4-year-old, (**B**) 40-year-old, and (**C**) 100-year-old fermentation cellars, using |Spearman's ρ| > 0.80, $p < 0.01$ and K-core ≥ 3. Nodes represent genera and colors indicate phylum. (**D**–**F**) Zi–Pi plots of the broader unfiltered genus graphs for the same age groups; dashed lines at Zi = 2.5 and Pi = 0.62 delimit peripheral nodes, connectors, module hubs, and network hubs. These networks are presented as exploratory descriptions.

3.4. Differences in Bottom Pit Mud Metabolite Profiles Among Cellar Age Groups

Nonvolatile metabolite profiles in bottom pit mud were characterized using untargeted LC–MS analysis. In total, 1939 metabolomic features were detected, of which 1869 passed quality control filtering. As shown in Figure 3A, lipids and lipid-like molecules (13.98%) and organic acids and derivatives (9.70%) were the largest assigned superclasses. Nucleosides, nucleotides, and analogues accounted for 2.53%, and 52.45% of features remained

unassigned at the superclass level. The fitted OPLS-DA model separated 4-B, 40-B, and 100-B (Figure 3B), with $R^2Y = 0.990$ and $Q^2 = 0.787$ (Figure 3C).

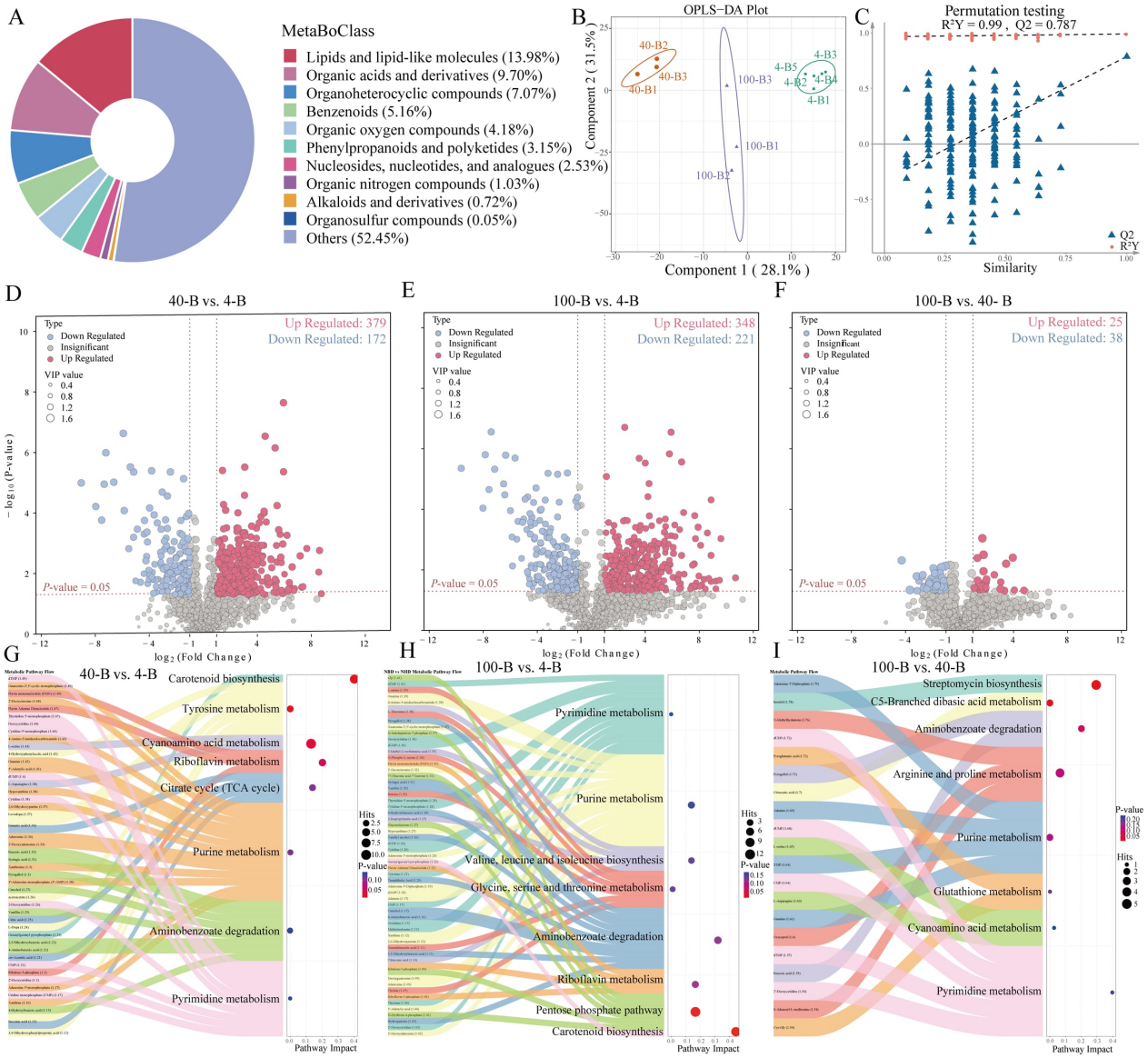

Figure 3. Metabolomic profiles and differential metabolite features in bottom pit mud across cellar ages. (**A**) Classification and relative proportions of annotated metabolite features. (**B**) Orthogonal partial least squares discriminant analysis (OPLS-DA) score plot for bottom samples from the three cellar age groups. (**C**) Permutation assessment of the discriminant model using R^2Y and Q^2 statistics. (**D**–**F**) Volcano plots for 40-B versus 4-B, 100-B versus 4-B, and 100-B versus 40-B, respectively. Features with a coefficient of variation greater than 30% across quality control samples were excluded from these comparisons. (**G**–**I**) Sankey diagram illustrating the KEGG pathway enrichment of differential metabolites among different comparisons. Corresponding metabolite names on the left are ordered by VIP value in descending order.

Following the exclusion of features with a coefficient of variation > 30% across quality control samples, differential metabolite features in bottom pit mud were screened using fold change (FC ≥ 2 or FC ≤ 0.5) and $p < 0.05$. As shown in Figure 3D–F, 551 differential features were identified in 40-B vs. 4-B, 569 in 100-B vs. 4-B, and 63 in 100-B vs. 40-B. Among features with assigned chemical classes, the largest assigned categories in 40-B vs. 4-B were lipids and lipid-like molecules (18.15%; 87 upregulated and 13 downregulated), organic acids and derivatives (6.90%; 21 upregulated and 17 downregulated). Similarly, lipids and

lipid-like molecules represented the largest assigned category in 100-B vs. 4-B (14.41%; 67 upregulated and 15 downregulated), followed by organic acids and derivatives (6.85%; 15 upregulated and 24 downregulated). In 100-B vs. 40-B, the largest assigned categories were lipids and lipid-like molecules (12.70%; 5 upregulated and 3 downregulated), organic acids and derivatives (11.11%; 1 upregulated and 6 downregulated).

Differential metabolites were further mapped to metabolic pathways using the KEGG database. In 40-B vs. 4-B, the mapped pathways included pyrimidine metabolism, purine metabolism, and aminobenzoate degradation, with additional mapping to the TCA cycle (Figure 3G). In 100-B vs. 4-B, pyrimidine and purine metabolism were accompanied by glycine, serine and threonine metabolism and the pentose phosphate pathway (Figure 3H). In 100-B vs. 40-B, the mapped pathways included pyrimidine metabolism, cyanoamino acid metabolism, glutathione metabolism, and arginine and proline metabolism (Figure 3I). Purine and pyrimidine metabolism were shared across all three comparisons, with common mapped features including guanine, dTMP, and dUMP. Aminobenzoate degradation was also represented in each comparison.

3.5. Associations of Microbial Communities with Environmental Factors and Metabolite Profiles

Redundancy analysis (RDA) with Monte Carlo permutation tests revealed significant associations between environmental factors and microbial community composition, with different environmental associations for bacteria, fungi and archaea. The bacterial RDA model explained 61.17% of total community variation ($p = 0.001$; Figure 4A), including 43.62% on the first two axes. TC, TN and TDN were associated with bacterial ordination. For fungi, BG, TPM, and AP were environmental variables associated with community composition. The model accounted for 54.25% of total variation ($p = 0.008$; Figure 4B), with the first two axes representing 28.96%. Environmental variables explained 43.20% of archaeal community variation ($p = 0.005$; Figure 4C), including 33.21% on the first two axes. POX, MBN, and PER were the environmental variables associated with the archaeal ordination.

Procrustes analysis detected significant concordance between environmental and bacterial community configurations ($M^2 = 0.6819$, $p = 0.0035$, $q = 0.0105$; Figure S4A). The corresponding comparisons were not significant for fungi ($M^2 = 0.8600$, $p = 0.1773$, $q = 0.1773$; Figure S4B) or archaea ($M^2 = 0.9252$, $p = 0.1376$, $q = 0.1773$; Figure S4C).

Among the associations displayed in Figure 4D–F, 21 bacterial and five fungal genus–environment correlations were significant. *Acetivibrio* was positively correlated with pH. DOC was positively correlated with *Lactobacillus* and negatively correlated with *Hydrogenispora*. *Leptolinea* was negatively correlated with AP and MBN, and *Prevotellamassilia* was negatively correlated with MBN. Among fungi, *Trichosporon* was positively correlated with DOD; *Monascus* was negatively correlated with microbial C:N. No displayed archaeal association met the adjusted threshold.

Random forest models identified TDN and MBN among the significant importance predictors of both bacterial Shannon diversity and bacterial PCoA1 scores in bottom samples (Figure S6). AP, CBH, and NAG were significant importance predictors of archaeal Shannon diversity and PCoA1 scores. In matched bottom samples, bacterial community composition was concordant with metabolite profiles ($M^2 = 0.3829$, $p = 0.0001$, $q < 0.001$; Figure S7B). The corresponding comparisons were not significant for fungi ($M^2 = 0.7929$, $p = 0.2510$, $q = 0.3765$; Figure S7C) or archaea ($M^2 = 0.9547$, $p = 0.9080$, $q = 0.9080$; Figure S7D). To further explore associations between microbial genera and environmental properties, elemental concentrations, and metabolite profiles, Mantel tests used BH-adjusted $q < 0.05$ for bacteria, fungi and archaea (Figure 5A–C). The strongest physicochemical associations involved *Sedimentibacter* with pH ($r = 0.338$), *Trichosporon* with DOD ($r = 0.297$), and *Methanosphaerula*

with HA (r = 0.257). DOC showed a shared association pattern across the three domains, linking to *Caproiciproducens* (r = 0.162), *Aspergillus* (r = 0.166), and *Methanothrix* (r = 0.232). For elemental concentrations, bacteria, fungi, and archaea exhibited 32, 10, and two associations, respectively. The strongest bacterial association involved *Proteiniphilum* and phosphorus (r = 0.778). Shared associations occurred between pairs of domains: manganese was associated with *Proteiniphilum* (r = 0.754) and *Trichosporon* (r = 0.360), and potassium was associated with *Aspergillus* (r = 0.402) and *Methanothermobacter* (r = 0.395). The remaining archaeal association involved *Methanosarcina* and molybdenum (r = 0.395).

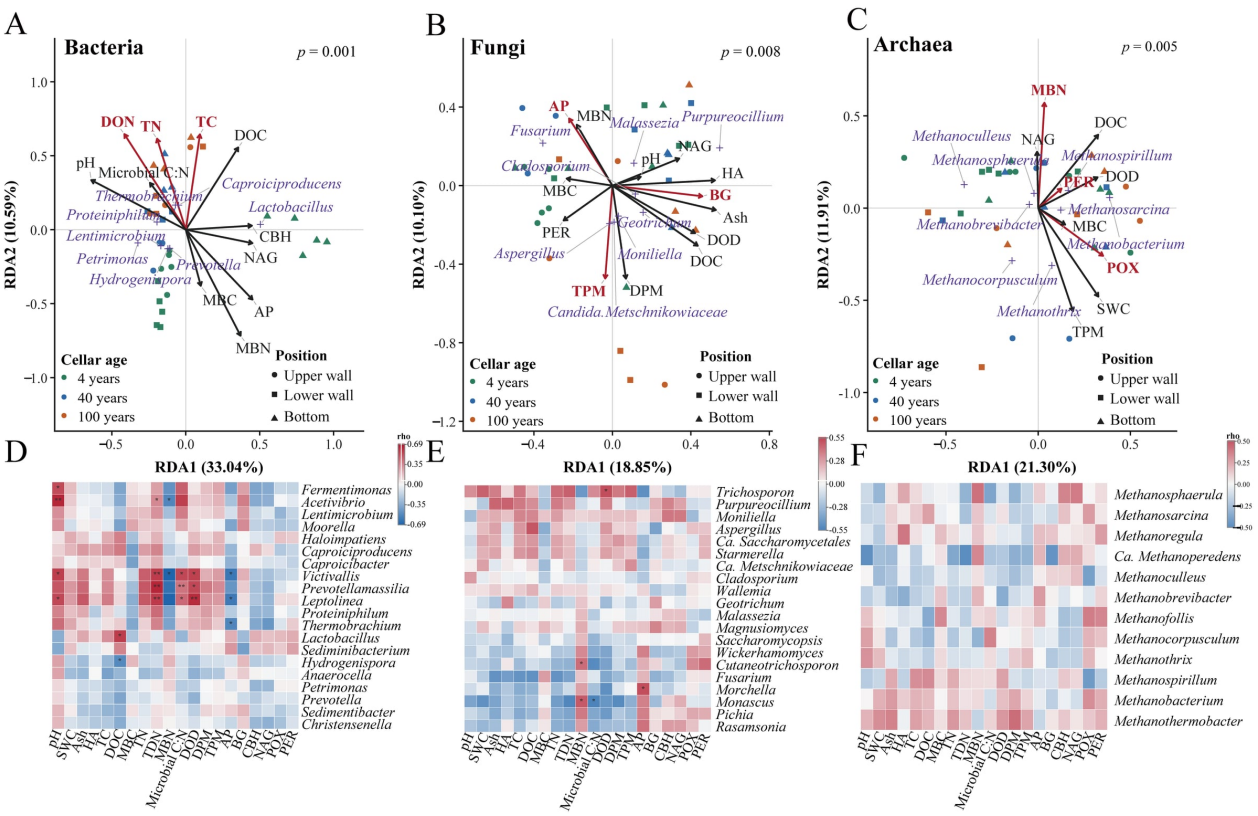

Figure 4. Associations between microbial community composition and environmental properties across cellar age groups and sampling positions. (**A**–**C**) Redundancy analysis (RDA) of bacterial, fungal, and archaeal communities, respectively, based on genus level community data and environmental measurements from 33 matched samples spanning all sampling positions. Point colors indicate cellar age groups, and point shapes indicate sampling positions. Environmental vectors and selected microbial genera are shown; highlighted environmental vectors are displayed in red. The *p* values refer to permutation tests of the corresponding RDA models. (**D**–**F**) Spearman correlation heatmaps linking bacterial, fungal, and archaeal genera, respectively, to environmental variables. *p* values were adjusted using the Benjamini–Hochberg procedure across all genus–environment tests from the three microbial domains. Asterisks indicate BH-adjusted probabilities: * $q < 0.05$ and ** $q < 0.01$.

A total of 54 metabolites were selected by considering differences among cellar age groups ($q < 0.05$ after BH correction across 1939 features), relevance to fermentation, and available annotation evidence. These metabolites yielded associations with bacteria (197), fungi (64), and archaea (26). Sixteen annotated metabolites were associated with genera in all three domains. The δ-tridecalactone was associated with *Sediminibacterium* (r = 0.906), *Pichia* (r = 0.481), and *Methanobrevibacter* (r = 0.478). Linoleic acid was associated with *Proteiniphilum* (r = 0.577), *Trichosporon* (r = 0.526), and *Methanospirillum* (r = 0.477). The strongest fungal association linked *Trichosporon* to S-lactoylglutathione (r = 0.764), and the

strongest archaeal association linked *Candidatus Methanoperedens* to hydrocinnamic acid ($r = 0.595$).

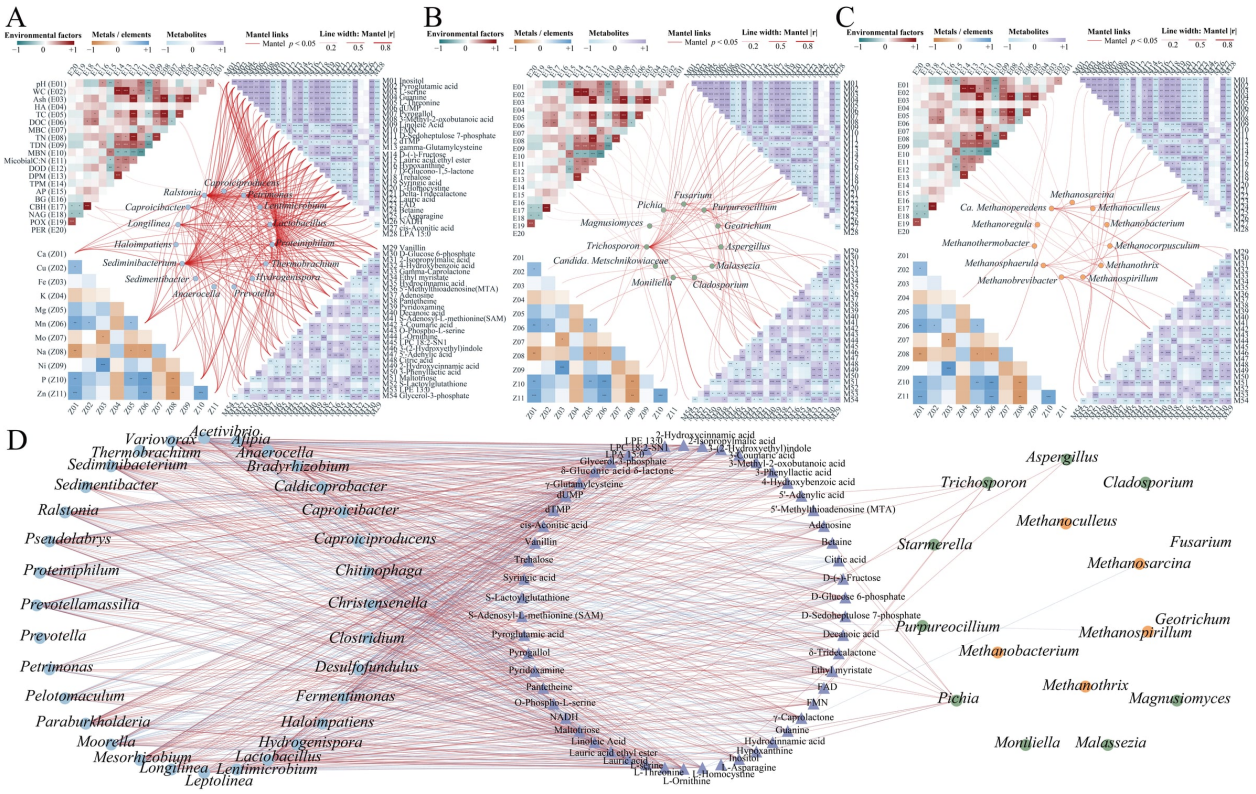

Figure 5. Associations of microbial genera with environmental variables and selected metabolites in pit mud. (**A**–**C**) Correlation matrices and genus level Mantel test for (**A**) bacterial, (**B**) fungal, and (**C**) archaeal communities. In each panel, the upper-left matrix contains 20 environmental variables measured across all sampling positions ($n = 33$), and the lower-left matrix contains 11 elemental variables measured in bottom samples ($n = 11$). Asterisks indicate unadjusted significance levels: * $p < 0.05$, ** $p < 0.01$, and *** $p < 0.001$. Displayed Mantel links meet Benjamini–Hochberg-adjusted $q < 0.05$. (**D**) Spearman correlation network linking microbial genera to metabolite features in bottom pit mud samples. Red and blue edges indicate positive and negative correlations, respectively, satisfying $|\rho| \geq 0.60$ and $p < 0.05$.

3.6. Integrative Modeling of Environmental–Microbial–Metabolite Associations in Bottom Pit Mud

Random forest regression identified potential environmental and microbial predictors of differential metabolite variation in bottom pit mud, explaining 70.36% of the out of bag variation in the metabolite profile response (Figure 6A). Na ranked highest among elemental predictors, and bacterial PCoA1 ranked highest among microbial predictors; both showed significant predictor importance. MBN and microbial biomass C:N also showed significant importance, but TN was not significant. Additional significant predictors included AP, CBH, bacterial Shannon diversity, and archaeal PCoA1.

Following this predictor screening, an exploratory PLS-PM linked cellar age, elemental concentrations, nitrogen status, selected genera and selected metabolites (Figure 6B; GOF = 0.756). Cellar age was positively associated with element concentrations and nitrogen pools (path coefficients: $\beta = 0.724$ and $\beta = 0.814$, respectively; both $p < 0.05$). Nitrogen pools were negatively associated with the selected microbial community construct ($\beta = -0.862$, $p < 0.05$). The microbial community construct was positively associated with the differential metabolite construct ($\beta = 0.952$, $p < 0.05$), representing the strongest direct path in the model. A sequential pattern linked cellar age, nitrogen pools, microbial

community composition, and differential metabolites. The model explained 79% of the variance in the microbial community construct and 90% of the variance in the differential metabolite construct (Figure 6B). Effect decomposition showed that the microbial community construct had the largest positive direct and total effects on the differential metabolite construct. Nitrogen pools had the largest negative indirect effect (Figure 6C).

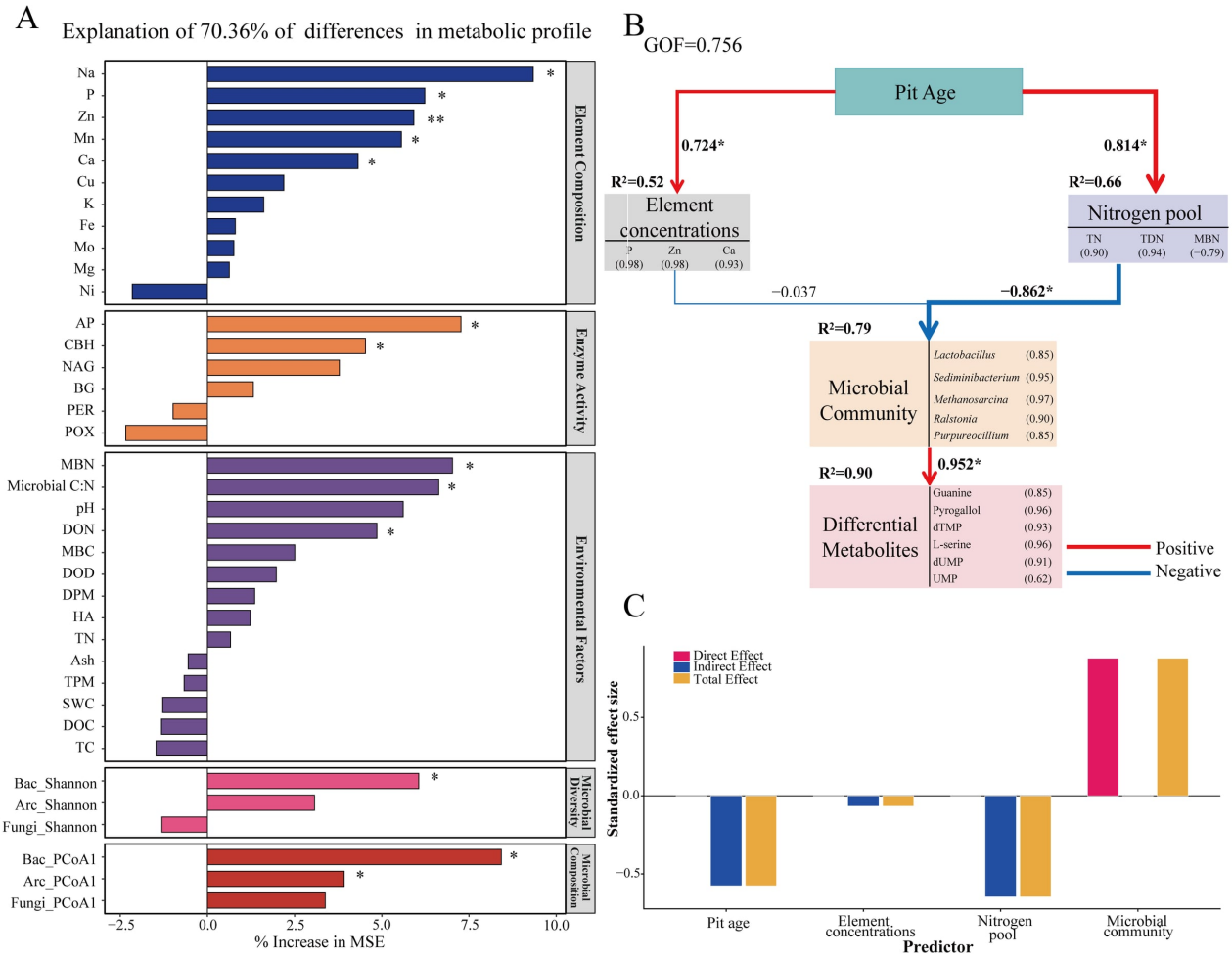

Figure 6. Random forest prediction and exploratory path modeling of environmental, microbial and metabolite associations in bottom pit mud. (**A**) Random forest importance of elemental concentrations, enzyme activities, environmental properties, microbial diversity, and community composition in predicting the first principal component of the metabolite profile. Asterisks indicate permutation-based importance p values: * $p < 0.05$ and ** $p < 0.01$. (**B**) Partial least squares structural equation model (PLS-SEM) representing the specified relationships among pit age, elemental concentrations, nitrogen pools, microbial community indicators, and selected metabolites. Asterisks indicate significant path coefficients based on 2000 bootstrap resamples: * $p < 0.05$. The GOF greater than 0.4 indicates that the model fits correctly. (**C**) Estimated standardized direct, indirect, and total effects of the displayed predictors on the metabolite construct.

4. Discussion

Cellar age and sampling position were associated with distinct physicochemical conditions in pit mud. The older cellars had higher pH and water content, and TC increased towards the bottom within each age group. DOC was consistently lowest at the upper wall. These spatial contrasts are relevant to the exchange of substrates between Jiupei and pit mud during repeated fermentation. Huangshui formation involves water movement through fermented grains [30], and its microbial and organic acid profiles vary with cellar age [31].

Differences in substrate delivery, retention, and consumption could therefore contribute to the resource conditions observed at different positions.

Higher TN and TDN coincided with lower MBN in both older groups at all three sampling positions. MBC showed a different spatial pattern, with higher concentrations in older mud at the upper wall but in young mud at the lower wall and bottom. At the bottom, the higher biomass C:N in older mud described less nitrogen relative to carbon in the estimated biomass. These observations distinguish bulk nitrogen enrichment from microbial biomass nitrogen status. The higher biomass C:N at the upper wall of 40-year cellars further indicates that biomass stoichiometry also varies with position, such that carbon-rich conditions can coincide with a nitrogen-poor biomass pool.

Several complementary processes may contribute to these patterns. Repeated fermentation inputs, nitrogen retention, and microbial turnover offer possible explanations for the contrast between nitrogen concentrations and MBN. Soil isotope experiments show that microbially derived nitrogen can persist in mineral associated fractions [32], and long term fertilization can produce different responses in accumulated microbial residues and standing biomass [33]. Experiments in soil and litter further demonstrate that carbon and nitrogen imbalance affects nitrogen incorporation and release [34,35]. These studies provide mechanisms to examine in pit mud. Repeated inputs could increase nitrogen retained in the matrix without a corresponding increase in the nitrogen represented in living biomass.

Bacterial differentiation was particularly evident at the bottom, where older mud had higher Shannon diversity, lower *Lactobacillus* relative abundance, and greater relative abundances of several anaerobic genera. The interactions between cellar age and position show that these taxonomic patterns were spatially dependent. RDA associated bacterial composition with TC, TN, and TDN (Figure 4A), consistent with previous pit mud surveys relating succession to nutrient conditions [36]. The community comparison also detected differences in dispersion, so the age pattern includes variation within groups as well as separation between groups. The concordance between bacterial composition and bottom metabolite profiles supports examining bacterial differentiation alongside nitrogen status.

Proteiniphilum, *Petrimonas*, and *Sedimentibacter* were more prominent in the relative composition of older bottom mud. Culture studies give a biological basis for investigating proteinaceous substrate use by some of these populations: *Proteiniphilum propionicum* grows on yeast extract, tryptone, and peptone, and *Sedimentibacter acidaminivorans* ferments several amino acids [37,38]. These traits motivate tests of how the enriched genera use nitrogenous resources during fermentation. In inoculated pit mud, increasing *Proteiniphilum* has also accompanied declines in caproate producers and fatty acid and ester concentrations [39].

Lactobacillus relative abundance declined at the bottom but increased at the lower wall of older cellars, although MBN was lower at both positions. Its compositional pattern therefore differed from the pattern of nitrogen in the whole microbial biomass. Amino acids supplied through microbial interactions can support growth of *Lactobacillus* in Baijiu fermentation [40]. Shannon diversity describes richness and evenness, and amplicon relative abundances describe sequence composition. Greater bacterial diversity and higher relative abundances of selected genera can therefore coexist with lower MBN.

Fungal profiles showed local taxonomic differences, but the overall age comparison was not significant after accounting for cellar replication. BG, TPM, and AP were associated with fungal ordination (Figure 4B). Experimental evidence linking amino acids to fungal assembly in Baijiu [6] supports examining these resource relationships. Archaeal ordination was associated with MBN, POX, and PER (Figure 4C). Genome studies and cocultures support complementary bacterial fermentation and archaeal methanogenesis in pit mud systems [41,42]. These comparisons provide targets for functional characterization. POX and PER represent oxidative potentials under the assay conditions.

Bottom metabolite profiles differed more between young mud and the older groups than between the two older groups. Lower signals for glucose 6-phosphate, sedoheptulose 7-phosphate, and trehalose accompanied lower serine, threonine, guanine, and dUMP signals; homocystine was higher in older mud. These directions describe chemical differentiation. Bulk nitrogen and individual metabolite signals represent different measurements. Inputs, synthesis, uptake, consumption, and exchange can all affect the residual profiles. The measured profiles therefore identify compounds and resource transformations for targeted investigation.

Methylthioadenosine was higher in 40-B. In Baijiu cultures, this compound, lysine, and methionine released by *Saccharomyces cerevisiae* have promoted *Lactobacillus panis* growth, with the interaction depending on reducing sugar conditions [43,44]. This provides a specific target for testing nitrogenous resource exchange in the carbon conditions of bottom pit mud.

Acids produced by fermented grain communities can support further organic acid formation by pit mud microorganisms [3]. Repeated exchange with Jiupei should therefore be considered when investigating the nitrogen and biomass contrasts. Carbon and nitrogen arrive in different chemical forms, and their release, transport, and utilization need not coincide with incorporation into biomass. Matched sampling of Jiupei, Huangshui, and pit mud across fermentation batches would test how these processes relate to the observed nitrogen patterns.

The integrative analyses highlighted MBN and biomass C:N alongside Na and bacterial composition as predictors of variation in the selected bottom metabolite features (Figure 6A). MBN and biomass C:N share information because MBN is the denominator of the ratio and should be interpreted jointly. In the exploratory path model, the nitrogen construct contrasted positive TN and TDN loadings with a negative MBN loading and was associated with the selected microbial and metabolite constructs (Figure 6B,C). Because the microbial and metabolite indicators were selected after examining age differences and paths were iteratively screened, the paths and explained variance describe this selected set.

For pit mud management, a high bulk nitrogen concentration does not describe the microbial biomass nitrogen pool. Joint measurement of TN, TDN, MBN, biomass C:N, and local habitat conditions can capture differences between young and older mud that a single nitrogen measurement would miss. Proteins, peptides, and amino acids supply resources to fermentation microorganisms [45], making input composition and the accompanying carbon resources relevant variables for management trials. These data identify measurements and populations to examine.

Interventions with simplified pit mud consortia or indigenous microbes have improved flavor profiles and, in some cases, sensory outcomes [46,47]. In this study, the candidate measurements concern nitrogen status and biochemical differentiation. Lower MBN can be monitored jointly with TN, TDN, and biomass C:N, and its links to liquor quality can be examined against matched acid, ester, and sensory profiles across fermentation batches. This provides a basis for production trials that link pit mud monitoring and maintenance to fermentation stability and Baijiu quality.

5. Conclusions

In summary, this study reveals distinct microbial responses across cellar ages and spatial positions and links nitrogen status with bottom metabolite differentiation in strong-flavor Baijiu pit mud. Bulk nitrogen enrichment and estimated microbial biomass nitrogen describe distinct dimensions of pit mud conditions. Their contrasting patterns and the spatial variation in biomass stoichiometry support assessing nitrogen status at individual cellar positions. Bacterial differentiation was most evident at the pit bottom and was as-

sociated with carbon and nitrogen conditions. Fungal variation mainly reflected spatial position, while dominant archaeal genera showed comparatively stable distributions. Bacterial composition also showed the clearest correspondence with bottom metabolite profiles, linking community differentiation with biochemical variation that included amino acid and nucleotide metabolites. Joint assessment of nitrogen pools, biomass stoichiometry and bacterial composition can help distillery personnel distinguish nutrient enrichment from microbial biomass status and select targets for pit mud monitoring. These measurements can inform nutrient management and maintenance trials aimed at improving fermentation stability and Baijiu quality consistency.

Supplementary Materials: The following supporting information can be downloaded at https://www.mdpi.com/article/10.3390/foods15234281/s1: Figure S1: Elemental concentrations in bottom pit mud across cellar age groups; Figure S2: Alpha diversity of bacterial, fungal, and archaeal communities across cellar ages and sampling positions; Figure S3: Inferred assembly processes of bacterial, fungal, and archaeal communities in pit mud; Figure S4: Procrustes comparisons between environmental and microbial community configurations for bacteria, fungi, and archaea; Figure S5: Spearman correlations between elemental concentrations and the relative abundances of bacterial, fungal, and archaeal genera in matched bottom pit mud samples; Figure S6: Random forest importance of environmental predictors for microbial diversity and community composition in bottom pit mud; Figure S7: Metabolite abundance patterns and their concordance with microbial community composition in bottom pit mud; Table S1: Relative abundances of dominant microbial genera across cellar ages and sampling positions and the effects of age, position, and their interaction.

Author Contributions: Methodology, T.H.; validation, T.H. and Z.L.; formal analysis, T.H.; investigation, Z.L., M.S. and B.D.; data curation, T.H. and M.S.; writing—original draft preparation, T.H.; writing—review and editing, D.X.; visualization, T.H.; supervision, H.C. and B.D.; project administration, H.C.; funding acquisition, H.C. and D.X. All authors have read and agreed to the published version of the manuscript.

Funding: This work was supported by the commissioned project from Luzhou Laojiao Co., Ltd. (GFGS-2022000550), the Youth Innovation Promotion Association of the Chinese Academy of Sciences (2022376) and the Natural Science Foundation of Sichuan Province (2025NSFJQ0028).

Institutional Review Board Statement: Not applicable.

Informed Consent Statement: Not applicable.

Data Availability Statement: Raw PacBio sequencing reads have been deposited in the Genome Sequence Archive (GSA) under accession CRA083736 (https://ngdc.cncb.ac.cn/gsa/browse/CRA083736, accessed on 10 October 2028). Metabolomics data have been deposited in the Open Archive for Miscellaneous Data (OMIX) under accession OMIX016615 (https://ngdc.cncb.ac.cn/omix/release/OMIX016615, accessed on 1 September 2028).

Acknowledgments: During the preparation of this manuscript, the authors used GPT-6 (OpenAI) to assist with text revision. The authors reviewed and edited the output and take full responsibility for the content of this publication.

Conflicts of Interest: Author Zongze Li was employed by the company National Engineering Research Center of Solid-state Brewing, Luzhou Laojiao Group Co., Ltd. He participated in Validation and investigation in the study. Author Min Sun was employed by the company National Engineering Research Center of Solid-state Brewing, Luzhou Laojiao Group Co., Ltd. She participated in investigation and data curation in the study. Author Bo Deng was employed by the company National Engineering Research Center of Solid-state Brewing, Luzhou Laojiao Group Co., Ltd. He participated in supervision and investigation in the study.The role of the company was project funding support. The remaining authors declare that the research was conducted in the absence of any commercial or financial relationships that could be construed as a potential conflict of interest.

References

1. Dai, M.; Niu, Z.; Lu, Y.; Wei, A.; Wang, X.; Zheng, H.; Lai, J.; Zong, E.; Sun, B.; Zheng, J.; et al. Unveiling the Acidic Backbone of Baijiu: A Comprehensive Review on Composition, Metabolic Pathways, and Quality Implications. *Compr. Rev. Food Sci. Food Saf.* **2026**, *25*, e70592. [CrossRef]
2. Zeng, Y.; Zhong, X.; Chai, L.; Zhang, X.; Lu, Z.; Liu, G.; Tu, T.; Lu, L.; Zhang, R.; Yu, H.; et al. Prokaryotic Evolution Shapes Specialized Communities in Long Term Engineered Pit Mud Ecosystem. *npj Biofilms Microbiomes* **2025**, *11*, 186. [CrossRef]
3. Qian, W.; Lu, Z.-M.; Chai, L.-J.; Zhang, X.-J.; Li, Q.; Wang, S.-T.; Shen, C.-H.; Shi, J.-S.; Xu, Z.-H. Cooperation within the Microbial Consortia of Fermented Grains and Pit Mud Drives Organic Acid Synthesis in Strong-Flavor Baijiu Production. *Food Res. Int.* **2021**, *147*, 110449. [CrossRef]
4. Dai, M.; Wang, X.; Wang, H.; Wu, M.; Lai, J.; Zong, E.; Zheng, J.; Xu, Y.; Sun, B. Butyrogenic and Caprogenic Bacteria from Pit Mud of Strong-Aroma Baijiu Engage in Mutualistic Cross-Feeding and Promoting Caproic Acid Biosynthesis. *Int. J. Food Microbiol.* **2025**, *443*, 111434. [CrossRef]
5. Xu, S.; Li, J.; Wang, F.; Bian, H.; Yan, W.; Wang, H.; Jiang, C.; Sun, J.; Wang, Z.; Li, X. Depth-Dependent Microbial Succession and Interspecies Hydrogen Transfer Drive Pit Mud Maturation in Chinese Strong-Flavor Baijiu Fermentation. *Food Res. Int.* **2026**, *243*, 120362. [CrossRef]
6. Wei, J.; Lu, J.; Nie, Y.; Li, C.; Du, H.; Xu, Y. Amino Acids Drive the Deterministic Assembly Process of Fungal Community and Affect the Flavor Metabolites in Baijiu Fermentation. *Microbiol. Spectr.* **2023**, *11*, e02640-22. [CrossRef]
7. Jones, D.L.; Willett, V.B. Experimental Evaluation of Methods to Quantify Dissolved Organic Nitrogen (DON) and Dissolved Organic Carbon (DOC) in Soil. *Soil Biol. Biochem.* **2006**, *38*, 991–999. [CrossRef]
8. Xu, X.; Thornton, P.E.; Post, W.M. A Global Analysis of Soil Microbial Biomass Carbon, Nitrogen and Phosphorus in Terrestrial Ecosystems. *Glob. Ecol. Biogeogr.* **2013**, *22*, 737–749. [CrossRef]
9. Buckeridge, K.M.; Mason, K.E.; Ostle, N.; McNamara, N.P.; Grant, H.K.; Whitaker, J. Microbial Necromass Carbon and Nitrogen Persistence Are Decoupled in Agricultural Grassland Soils. *Commun. Earth Environ.* **2022**, *3*, 114. [CrossRef]
10. Tao, Y.; Li, J.; Rui, J.; Xu, Z.; Zhou, Y.; Hu, X.; Wang, X.; Liu, M.; Li, D.; Li, X. Prokaryotic Communities in Pit Mud from Different-Aged Cellars Used for the Production of Chinese Strong-Flavored Liquor. *Appl. Environ. Microbiol.* **2014**, *80*, 2254–2260. [CrossRef]
11. Ren, D.; Liu, S.; Qin, H.; Huang, M.; Han, X.; Zhang, S.; Mao, J. Heterogenetic Mechanism in Multidimensional Pit Mud with Different Fermentation Years: From Microbial Structure Dynamic Succession to Metabolism Phenotypes. *Food Res. Int.* **2024**, *192*, 114770. [CrossRef]
12. Wen, Z.; Wei, Y.-H.; Han, D.-Y.; Song, L.; Zhu, H.-Y.; Guo, L.-C.; He, C.-J.; Guo, Z.-X.; Han, P.-J. Effects of Pit Mud on the Spatial Heterogeneity of Bacterial Communities and Volatile Metabolites in Jiupei: Insights from Volatile Metabolomics and Microbial Community Analysis. *J. Agric. Food Res.* **2026**, *29*, 103067. [CrossRef]
13. Fernandes, R.B.A.; de Carvalho Junior, I.A.; Ribeiro Junior, E.S.; Mendonça, E.d.S. Comparison of Different Methods for the Determination of Total Organic Carbon and Humic Substances in Brazilian Soils. *Rev. Ceres* **2015**, *62*, 496–501. [CrossRef]
14. Zhao, H.; O'Connor, J.; Zou, S.; Solaiman, Z.M.; Mickan, B.S.; Bolan, N. Soil Health and Carbon Storage in Community Gardens in the Perth Metropolitan Area, Australia. *Soil Use Manag.* **2024**, *40*, e13033. [CrossRef]
15. *GB/T 34766-2017*; Determination of Total Humic Acid Content from Mineral Source. China Standards Press: Beijing, China, 2017.
16. Wang, H.; Tian, J.; Chen, H.; Ho, M.; Vilgalys, R.; Bu, Z.-J.; Liu, X.; Richardson, C.J. Vegetation and microbes interact to preserve carbon in many wooded peatlands. *Commun. Earth Environ.* **2021**, *2*, 67. [CrossRef]
17. McGivern, B.B.; Cronin, D.R.; Ellenbogen, J.B.; Borton, M.A.; Knutson, E.L.; Freire-Zapata, V.; Bouranis, J.A.; Bernhardt, L.; Hernandez, A.I.; Flynn, R.M.; et al. Microbial Polyphenol Metabolism Is Part of the Thawing Permafrost Carbon Cycle. *Nat. Microbiol.* **2024**, *9*, 1454–1466. [CrossRef]
18. Wang, H.; Hong, Y.; Zhu, Y.; Hong, B.; Lin, Q.; Xu, H.; Leng, X.; Mao, X. Humification degrees of peat in Qinghai-Xizang Plateau and palaeoclimate change. *Chin. Sci. Bull.* **2004**, *49*, 514–519. [CrossRef]
19. Brookes, P.C.; Landman, A.; Pruden, G.; Jenkinson, D.S. Chloroform Fumigation and the Release of Soil Nitrogen: A Rapid Direct Extraction Method to Measure Microbial Biomass Nitrogen in Soil. *Soil Biol. Biochem.* **1985**, *17*, 837–842. [CrossRef]
20. Vance, E.D.; Brookes, P.C.; Jenkinson, D.S. An Extraction Method for Measuring Soil Microbial Biomass C. *Soil Biol. Biochem.* **1987**, *19*, 703–707. [CrossRef]
21. Saiya-Cork, K.R.; Sinsabaugh, R.L.; Zak, D.R. The Effects of Long Term Nitrogen Deposition on Extracellular Enzyme Activity in an *Acer Saccharum* Forest Soil. *Soil Biol. Biochem.* **2002**, *34*, 1309–1315. [CrossRef]
22. Yuan, M.; Breitkopf, S.B.; Yang, X.; Asara, J.M. A Positive/Negative Ion-Switching, Targeted Mass Spectrometry-Based Metabolomics Platform for Bodily Fluids, Cells, and Fresh and Fixed Tissue. *Nat. Protoc.* **2012**, *7*, 872–881. [CrossRef]
23. Wang, Q.; Garrity, G.M.; Tiedje, J.M.; Cole, J.R. Naïve Bayesian Classifier for Rapid Assignment of rRNA Sequences into the New Bacterial Taxonomy. *Appl. Environ. Microbiol.* **2007**, *73*, 5261–5267. [CrossRef]
24. Guimerà, R.; Nunes Amaral, L.A. Functional Cartography of Complex Metabolic Networks. *Nature* **2005**, *433*, 895–900. [CrossRef]

25. Sloan, W.T.; Lunn, M.; Woodcock, S.; Head, I.M.; Nee, S.; Curtis, T.P. Quantifying the Roles of Immigration and Chance in Shaping Prokaryote Community Structure. *Environ. Microbiol.* **2006**, *8*, 732–740. [CrossRef]
26. Dini-Andreote, F.; Stegen, J.C.; van Elsas, J.D.; Salles, J.F. Disentangling Mechanisms That Mediate the Balance between Stochastic and Deterministic Processes in Microbial Succession. *Proc. Natl. Acad. Sci. USA* **2015**, *112*, E1326–E1332. [CrossRef]
27. Stegen, J.C.; Lin, X.; Fredrickson, J.K.; Chen, X.; Kennedy, D.W.; Murray, C.J.; Rockhold, M.L.; Konopka, A. Quantifying Community Assembly Processes and Identifying Features That Impose Them. *ISME J.* **2013**, *7*, 2069–2079. [CrossRef]
28. Price, M.N.; Dehal, P.S.; Arkin, A.P. FastTree 2—Approximately Maximum-Likelihood Trees for Large Alignments. *PLoS ONE* **2010**, *5*, e9490. [CrossRef]
29. Tenenhaus, M.; Vinzi, V.E.; Chatelin, Y.-M.; Lauro, C. PLS Path Modeling. *Comput. Stat. Data Anal.* **2005**, *48*, 159–205. [CrossRef]
30. Ren, Z.; Chen, Q.; Tang, T.; Huang, Z. Unraveling the Water Source and Formation Process of Huangshui in Solid-State Fermentation. *Food Sci. Biotechnol.* **2025**, *34*, 665–675. [CrossRef]
31. Liu, Q.; Mei, J.; Wen, X.; Lu, Y.; Zeng, Y.; Liu, Z.; Xu, H.; Wang, S.; Jiang, F.; Yang, C.; et al. Cellar Age Reshapes Huangshui Micro-Ecosystem and Metabolism to Drive Flavor Formation in Strong-Aroma Baijiu. *Food Res. Int.* **2026**, *241*, 119740. [CrossRef]
32. Wang, X.; Wang, C.; Fan, X.; Sun, L.; Sang, C.; Wang, X.; Jiang, P.; Fang, Y.; Bai, E. Mineral Composition Controls the Stabilization of Microbially Derived Carbon and Nitrogen in Soils: Insights from an Isotope Tracing Model. *Glob. Chang. Biol.* **2024**, *30*, e17156. [CrossRef]
33. Schwalb, S.A.; Hemkemeyer, M.; Christensen, B.T.; Heinze, S.; Oliva, R.L.; Joergensen, R.G.; Wichern, F. Disentangling the Effects of Mineral Fertiliser N, P and K on Microbial Biomass, Necromass and Ionome in Soil from the Askov Long-Term Field Experiment. *Soil Biol. Biochem.* **2024**, *195*, 109449. [CrossRef]
34. Mooshammer, M.; Wanek, W.; Hämmerle, I.; Fuchslueger, L.; Hofhansl, F.; Knoltsch, A.; Schnecker, J.; Takriti, M.; Watzka, M.; Wild, B.; et al. Adjustment of Microbial Nitrogen Use Efficiency to Carbon:Nitrogen Imbalances Regulates Soil Nitrogen Cycling. *Nat. Commun.* **2014**, *5*, 3694. [CrossRef]
35. Sun, L.; Qiao, Y.; Wanek, W.; Moorhead, D.L.; Cui, Y.; Peng, Y.; Song, L.; Hu, B.; Zhang, T.; Li, S. Nitrogen Input Decreases Microbial Nitrogen Use Efficiency in Surface Soils of a Temperate Forest in Northeast China. *Geoderma* **2025**, *453*, 117159. [CrossRef]
36. Xia, H.; Jin, Y.; Zhao, D.; Zhou, R.; Zheng, J.; Wu, C. Mining the Factors Driving the Succession of Microbial Community in Pit Mud Used for the Production of Nongxiangxing Baijiu. *LWT* **2024**, *195*, 115806. [CrossRef]
37. Liu, Q.; Zheng, H.; Wang, H.; Zhou, W.; Zhao, D.; Qiao, Z.; Zheng, J.; Ren, C.; Xu, Y. *Proteiniphilum Propionicum* Sp. Nov., a Novel Member of the Phylum Bacteroidota Isolated from Pit Clay Used to Produce Chinese Liquor. *Int. J. Syst. Evol. Microbiol.* **2022**, *72*, 005612. [CrossRef]
38. Imachi, H.; Sakai, S.; Kubota, T.; Miyazaki, M.; Saito, Y.; Takai, K. *Sedimentibacter Acidaminivorans Sp. Nov.*, an Anaerobic, Amino-Acid-Utilizing Bacterium Isolated from Marine Subsurface Sediment. *Int. J. Syst. Evol. Microbiol.* **2016**, *66*, 1293–1300. [CrossRef]
39. Zhou, H.; Xu, S.; Xu, B.; Jiang, C.; Zhao, E.; Xu, Q.; Hong, J.; Li, X. Effect of *Caproicibacterium Lactatifermentans* Inoculation on the Microbial Succession and Flavor Formation of Pit Mud Used in Chinese Baijiu Fermentation. *Food Res. Int.* **2024**, *175*, 113730. [CrossRef]
40. Lin, L.; Du, R.; Wang, Y.; Wu, Q.; Xu, Y. Regulation of Auxotrophic Lactobacilli Growth by Amino Acid Cross-Feeding Interaction. *Int. J. Food Microbiol.* **2022**, *377*, 109769. [CrossRef]
41. Li, Z.; Zhao, C.; Mao, Z.; Zhang, F.; Dong, L.; Song, C.; Chen, Y.; Fu, X.; Ao, Z.; Xiong, Y.; et al. Structure and Metabolic Function of Spatiotemporal Pit Mud Microbiome. *Environ. Microbiome* **2025**, *20*, 10. [CrossRef]
42. Yan, S.; Dong, D. Improvement of Caproic Acid Production in a *Clostridium Kluyveri* H068 and Methanogen 166 Co-Culture Fermentation System. *AMB Express* **2018**, *8*, 175. [CrossRef]
43. Zhou, H.; Yan, L.; Xu, B.; Zhang, L.; Wang, R.; Chen, Q.; Li, X. Heterogeneous Selection Driven by pH Determines the Successional Pattern of Bacterial Communities in Pit Mud Used for Baijiu Fermentation. *Int. J. Food Microbiol.* **2026**, *450*, 111661. [CrossRef]
44. Liu, Y.; Wan, B.; Yang, F.; Zhang, X.; Li, J.; Du, G.; Wang, L.; Chen, J. Metabolomics-Driven Elucidation of Interactions between *Saccharomyces Cerevisiae* and *Lactobacillus Panis* from Chinese Baijiu Fermentation Microbiome. *Fermentation* **2022**, *8*, 33. [CrossRef]
45. Sun, H.; Ni, B.; Yang, J.; Qin, Y. Nitrogenous Compounds and Chinese Baijiu: A Review. *J. Inst. Brew.* **2022**, *128*, 5–14. [CrossRef]
46. Gao, J.; Qin, J.; Ye, F.; Ding, F.; Liu, G.; Li, A.; Ren, C.; Xu, Y. Constructing Simplified Microbial Consortia to Improve the Key Flavour Compounds during Strong Aroma-Type Baijiu Fermentation. *Int. J. Food Microbiol.* **2022**, *369*, 109594. [CrossRef]
47. Liu, M.-K.; Liu, C.-Y.; Tian, X.-H.; Feng, J.; Guo, X.-J.; Liu, Y.; Zhang, X.-Y.; Tang, Y.-M. Bioremediation of Degraded Pit Mud by Indigenous Microbes for Baijiu Production. *Food Microbiol.* **2022**, *108*, 104096. [CrossRef]

Disclaimer/Publisher's Note: The statements, opinions and data contained in all publications are solely those of the individual author(s) and contributor(s) and not of MDPI and/or the editor(s). MDPI and/or the editor(s) disclaim responsibility for any injury to people or property resulting from any ideas, methods, instructions or products referred to in the content.